Magnetic transitions in ultra-small nanoscopic magnetic rings: Theory and experiments

Deepak K. Singh, Robert Krotkov, and Mark T. Tuominen
Department of Physics, University of Massachusetts, Amherst, Massachusetts 01003, USA
(Received 27 May 2008; published 7 May 2009)

In this paper, we report on experimental and theoretical investigations of magnetic transitions in cobalt rings of size (diameter, width and thickness) comparable to the exchange length of cobalt. Magnetization measurements and calculations were performed for two sets of magnetic ring arrays: ultra-small magnetic rings (outer diameter 13 nm, inner diameter 5 nm and thickness 5 nm) and small magnetic rings (outer diameter 150 nm, width 5 nm, and thickness 5 nm). Our calculations suggest that if the linear dimensions of a magnetic ring are comparable to, or smaller than, the exchange length of the magnetic material, then only one magnetic state is important—the pure single-domain state. Vortex and onion-shape magnetic states do not arise. For a ring of larger diameter, magnetization reversal at zero field occurs via a vortex state. Theoretical calculations are based on an energetic analysis of pure and slightly distorted single-domain and vortex magnetic states. The calculations have been verified by micromagnetic simulations for ultra-small and small ring geometries. The hysteresis curves measured for small rings are consistent with the calculations, but there is a discrepancy for ultra-small rings. Micromagnetic simulations suggest that the discrepancies may be due to the variations in the shape and size of the ultra-small rings in the measured sample.

DOI: 10.1103/PhysRevB.79.184409 PACS number(s): 75.75.+a, 81.16.−c, 75.60.Ej

I. INTRODUCTION

In recent times, the magnetic ring geometry has been extensively studied, mostly because of its possible applications in magnetic memory devices. The application in memory devices is mostly driven by the fact that near zero-field value, a narrow nanoscopic magnetic ring can be in a flux closure vortex magnetic state.[1–3] A magnetic ring in vortex state has zero total magnetization and therefore each ring in an array acts like an individual memory element. Ring geometry is used in at least one current design of magnetic random access memory (MRAM).[4]

In addition to the vortex magnetic state, a small magnetic ring also forms two other stable magnetic states: the "onion state," characterized by the presence of two head-to-head domain walls, and the single-domain (SD) state, as shown in Fig. 1.[5] If the ring's width and thickness are comparable to the characteristic length (exchange length) of the parent magnetic material then the magnetic transition processes between these states are expected to be different from those in relatively larger size nanoscopic rings (~100 nm). We have found that if the ring sizes (diameter, width, and thickness) are sufficiently small then vortex and onion magnetic states have higher energies and do not arise. Therefore, magnetic transition processes in such ultra-small rings (outer diameter 13 nm) involve only saturating SD states. In the case of small rings (outer diameter 150 nm), having width and thickness comparable to those of ultra-small rings, the magnetic transition process is different: it occurs between two saturating SD states via the formation of vortex state near zero field. These conclusions are based on the calculation of total magnetic energies for various possible magnetic states and the measurement of magnetization as a function of applied field.

Due to the circular geometry of rings, shape anisotropy is absent; if the parent magnetic material is of polycrystalline origin then magnetocrystalline anisotropy is limited to random grains and can also be ignored.[6] For polycrystalline magnetic rings at zero field, the only competing energy terms are magnetostatic energy and quantum-mechanical exchange energy.[7,8] Exchange energy favors the parallel alignment of spins while the magnetostatic energy favors the circular magnetization.

In this paper, we present a study of magnetization and magnetic transitions in ultra-small and small polycrystalline magnetic, Co, rings of width and thickness comparable to the exchange length of Co (l_{ex}=3.8 nm).[9] The outline of this paper is as follows: first we discuss the fabrication of ultra-small and small ring arrays. The magnetic rings are fabricated using copolymer template, angular metal deposition, and ion-beam etching technique. Using this fabrication technique, we have been able to fabricate arrays of rings at two geometrical scales: ultra-small rings with outer diameter 13 nm, ring width 4 nm, and thickness ~5 nm and small rings with outer diameter 150 nm, ring width 5 nm and thickness ~5 nm. In the following sections, magnetization measurements of both ultra-small and small rings arrays are discussed. Experimental data are compared with detailed theoretical calculations for these rings. The theoretical calculations are based on the energetic analysis of possible magnetic states with the underlying assumption that only the lowest energy magnetic states will be excited. Different magnetic states in a ring structure are obtained using reasonable models of magnetization distortion on the ring's circumferences. Finally, experimental and theoretical results are discussed along with micromagnetic simulations in Sec. V.

II. FABRICATION PROCEDURE

Recently small ferromagnetic rings have been fabricated by electron-beam lithography,[1,10] evaporation over spheres,[11] and other methods.[12,13] Our nanoring fabrication technique is described in detail in an earlier work.[14] The fabrication process for both ultra-small and small rings involves the cre-

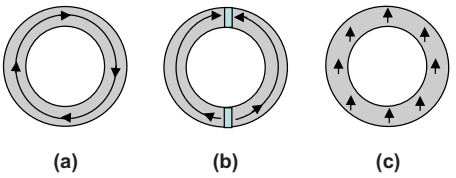

FIG. 1. (Color online) Magnetic states of nanorings. (a) Vortex magnetic state. (b) Onion magnetic state, with domain walls. (c) Single-domain magnetic state.

ation of a nanoporous polymer templates, angular deposition of desired material, Co, onto the wall of the pores and ion-beam etching technique to remove undesired material from the top of the template. In the case of ultra-small rings, the template is created from a self-assembled diblock copolymer film[15] which was 36 nm thick and had pores of average diameter 13 nm, separated by 28 nm. In the case of small rings, the template is created by electron-beam lithography technique[16] using 40 nm thick copolymer film PMMA [poly(methyl-metha-acrylate)]. In the case of copolymer PMMA film, the pore size was 150 nm and the separation between pores (center-to-center distance) was 350 nm.

The angular deposition of the desired material onto the walls of the nanopores was the most critical step of this fabrication scheme. During the angular deposition process, the substrate (a thin silicon wafer with polymer template on it) was uniformly rotated about the axis perpendicular to its plane. Angular deposition depends on a critical deposition angle $\theta_c = \tan^{-1}(D/h)$, where D and h are the diameter and height of the nanopore, respectively. In our experiment $D = 13$ nm and $h = 36$ nm for the fabrication of ultra-small rings and $D = 150$ nm and $h = 40$ nm for small rings, resulting in the critical angles of $\theta_c \sim 20°$ and 75°, respectively. Angles of $\theta = 23°$ and 75° were chosen for the fabrication of ultra-small and small rings, respectively. The thickness of deposited Co material on the walls of nanopores was in the range of 4–5 nm (based on the calibrated quartz-crystal microbalance reading). After material (cobalt) deposition, calibrated ion-beam etching was used to get the desired thicknesses of both ultra-small and small rings. The desired resulting thicknesses of both ultra-small and small rings were ~5 nm.

After ion-beam etching, the small ring samples were rinsed in acetone solvent to remove the remaining polymer residues and characterized by a field-emission scanning electron microscope (FESEM) (Fig. 2). Structural characterization of ultra-small rings was done using transmission electron microscope (TEM) (Fig. 2). Sample preparation of ultra-small rings for TEM imaging involved the transfer of ring templates onto electron transparent substrates. It was a difficult process and can be found in detail elsewhere.[14] The transfer of ring templates on electron transparent substrates also resulted in the loss of rings. For the magnetic measurement process, ultra-small rings were not transferred to an electron transparent substrate.

III. MAGNETIZATION MEASUREMENTS AND DATA ANALYSIS

Magnetic measurements of ultra-small and small rings arrays were carried out in a superconducting quantum interference device (SQUID) magnetometer with base temperature 1.8 K and with the applied field in the plane of the rings. Figures 3 and 4 show magnetization measurements at $T = 2$ K and $T = 300$ K for arrays of ultra-small and small rings, respectively. The data shown have been corrected for a linear diamagnetic background arising from the thin silicon wafer (500 μm). No magnetic hysteresis was observed in magnetization measurements at room temperature, 300 K.

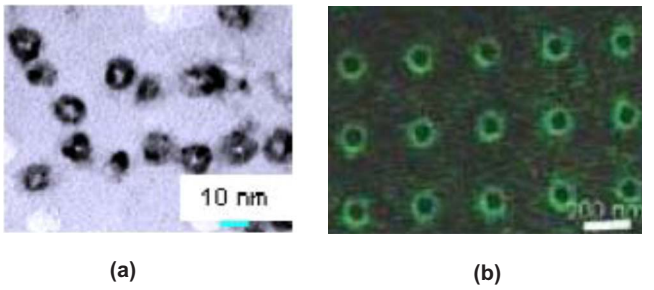

FIG. 2. (Color online) Images of rings. (a) TEM image of ultra-small rings and some empty diblock pores (rings came out of these pores during sample preparation for imaging). (b) FESEM images of small rings with thin wall.

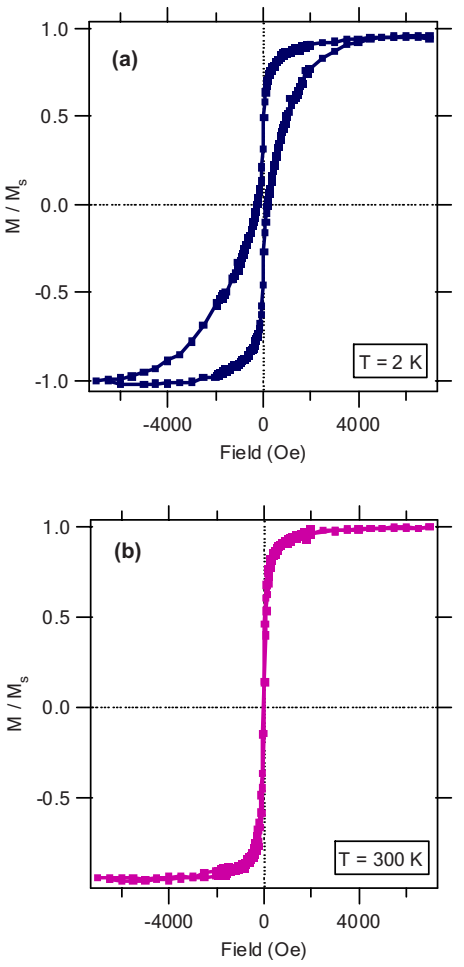

FIG. 3. (Color online) In-plane magnetization measurements for an array of ultra-small Co rings. (a) Measurements at 2 K. (b) Measurement at 300 K.

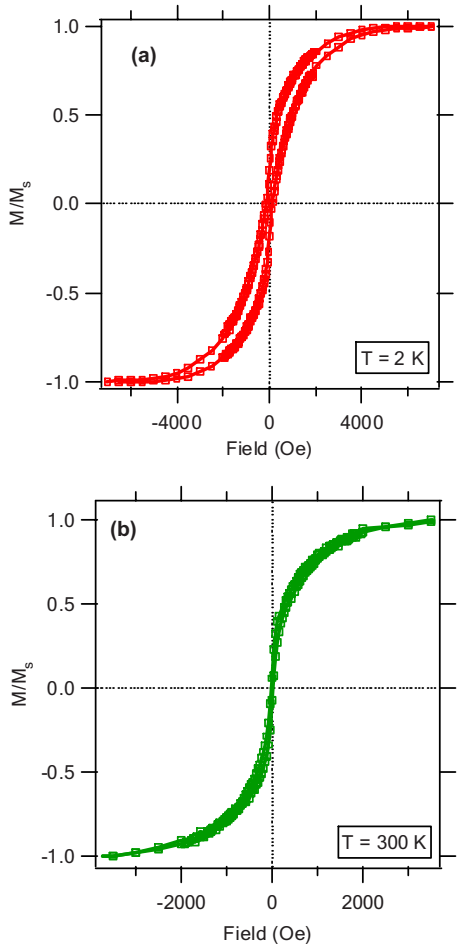

FIG. 4. (Color online) (a) Magnetization measurements data for small rings at 2 K. (b) Magnetic measurement at 300 K.

For arrays of ultra-small rings, the coercivity drops to zero above 20 K (data not shown here). Since interesting magnetization behaviors were observed only at low temperature (2 K), where thermal fluctuations are negligible, the remainder of the paper will focus on interpreting the low-temperature magnetization data.

As we can see in Figs. 3(a) and 4(a), the hysteresis curve is narrower near zero-field value than it is at saturation. Similar behavior is observed in nanoscopic narrow rings.[17] In relatively larger size nanoscopic rings, it is observed that the magnetic state is a single-domain state at saturation and as the field is decreased, the ring's magnetic state transforms to an "onion shape," and finally forms the flux closure vortex state near zero field (Fig. 1).[3,4] In general, magnetic transition processes in a small magnetic ring depend on the ring's diameter, width, thickness and ferromagnetic exchange length.[18]

In order to understand the magnetization data, shown in Figs. 3 and 4, and also to see if the magnetic transition processes in these cases are similar to what was observed for nanoscopic narrow rings, we calculate the total energy of a cobalt ring for possible magnetic states as a function of applied field. For any shape of body, those magnetic configurations which are energetically favored are dominant in determining the magnetic behavior.[5] In general, the magnetic state of a ring will be determined by the competition between exchange energy, magnetostatic energy, Zeeman energy, and magnetocrystalline energy. The exchange energy contribution favors the parallel alignment of the local magnetization **m** over the entire body while magnetostatic energy favors configurations where the magnetization follows a closed path inside the body, so that no net magnetic moment is produced.

As mentioned before, a magnetic ring exhibits three magnetic states in general: the uniformly magnetized SD state, the onion state, and the flux closure vortex state (Fig. 1). We calculate the energies of these three states as functions of applied field. For this purpose, we first consider an ultra-small ring. Since the thickness (5 nm) and width (4 nm) of the ultra-small ring are comparable to the exchange length, l_{ex}, of Co material (l_{ex}=3.8 nm),[9,19] magnetocrystalline anisotropy can be ignored for simplicity. For an ultra-small ring, the energetic analysis described below shows that only single-domain states are of significance at fields near zero; the energies of onion and vortex states lie above. An important underlying assumption in the calculation of energy is that since the thickness and width of the ring are comparable to the exchange length for cobalt, there is no variation in magnetization along the easy axis of the ring i.e., the magnetization pattern is purely two-dimensional in nature.

In dimensionless form, the free energy for a magnetic system of volume V is given by[19]

$$E = E_{ex} + E_{an} + E_m + E_{zeeman}$$
$$= \frac{1}{V}\int \left[\frac{l_{ex}^2}{2}(\nabla m^2) + \kappa f(m) - \frac{1}{2}(h_m \bullet m) - h_a \bullet m \right] d^3r.$$

Here M_s is the saturation magnetization of the material and $m=M/M_s$. $h_m=H_M/M_s$ and $h_a=H_a/M_s$ are dimensionless magnetic fields. H_a is the applied magnetic field, and H_M is the magnetic field produced by the magnetization of the sample. Energy is measured in units of $\mu_0 M_s^2 V$ therefore E =(Energy/$\mu_0 M_s^2 V$) is a dimensionless quantity. κ =$2K_1/\mu_0 M_s^2 = H_{an}/M_s$, where K_1 is the first crystalline anisotropy constant (which is taken to be zero for simplicity). The exchange length $l_{ex}=\sqrt{(2A/\mu_0 M_s^2)}$, where A is the exchange stiffness constant. Numerical values of relevant parameters are following: $M_s=1400\times10^3$ A/m, l_{ex}=3.8 nm, and h_a is the ratio of the applied field in A/m to 1400×10^3 A/m (which corresponds to 18000 Oe). Geometrical parameters for ultra-small and small ring are: R_1 (inner radius, ultra-small ring)=2.5 nm, R_2 (outer radius, ultra-small ring)=6.5 nm, t (thickness, ultra-small ring) =4 nm, R_1 (inner radius, small ring)=70 nm, R_2 (outer radius, small ring)=75 nm and t (thickness, small ring)=5 nm.

For the uniformly magnetized SD state, the exchange energy is zero and the total energy is the sum of the magnetostatic and Zeeman contributions.

$$E_{SD} = E_m + E_{zeeman}, \quad (1)$$

$$= 0.2 - h_a. \quad (2)$$

In the above equation, the dimensionless magnetostatic energy E_m=0.20 was obtained by numerical integration of the

energy density, which may be written as half the product of (magnetic) charge density and magnetostatic potential. The (surface) charge density was taken to be that of two oppositely charged ribbons on the ring's inner and outer surfaces, while the volume charge density is zero. We calculate the magnetostatic potential at an arbitrary point of the ring and then numerically integrate the energy density over the two ribbons.

For the vortex state, the magnetostatic, domain wall, and Zeeman energy contributions are all zero. Therefore, the total energy is solely exchange energy and is independent of the applied field. The exchange energy may be calculated analytically.

$$E_{vortex} = E_{ex}, \tag{3}$$

$$= \frac{l_{ex}^2}{R_2^2 - R_1^2} \ln \frac{R_2}{R_1}. \tag{4}$$

To calculate the energy of the onion configuration, we separate it into two parts: the ring arms and the domain walls (DW). The contributing energy terms are exchange, Zeeman, and magnetostatic. Exchange energy density is proportional to $\nabla \mathbf{m}^2$, so the vortex state and the ring arms of the onion state have the same exchange energy. The Zeeman energy is proportional to the cosine of the angle between the applied field and a line joining the two domain walls. The energy of onion magnetic state is

$$E_{onion} = E_{ex} + E_{zeeman} + E_{m(ringarms)} + E_{\mathrm{DW}}$$
$$= \frac{l_{ex}^2}{R_2^2 - R_1^2} \ln\left(\frac{R_2}{R_1}\right) - \frac{2}{\pi}[h_a] + E_{m(ringarms)} + E_{\mathrm{DW}}.$$

The line joining the domain walls has been taken to be in the direction of the applied field. Both $E_{m(ringarms)}$ and E_{DW} are positive: each increases the total energy of the onion state.

The energies of the SD and vortex states, together with a lower limit to the onion state energy, are plotted as functions of the dimensionless applied field h_a in Fig. 5. The lower limit is obtained by neglecting the domain wall and magnetostatic terms. If the domain walls were not lined up with the applied field, the slope of the onion curve would be smaller in magnitude. This figure suggests that at a given applied field the energy landscape has three local minima, with the SD state being lowest in energy. As the applied field is swept through zero, the vortex and onion magnetic states are not excited. Hence the corresponding magnetic hysteresis curve would correspond to a transition from one SD state to another SD state of opposite polarity, possibly by a uniform rotation of magnetic spins.

We have also carried out similar energy calculations for small rings. As mentioned in the fabrication section, a small ring's width (5 nm) and thickness (5 nm) are comparable to those of an ultra-small ring and therefore comparable to the exchange length of Co. However, the outer diameter of a small ring (150 nm) is an order of magnitude larger than the diameter of an ultra-small ring (13 nm). Based on the energy calculations, the calculated energies of the SD, onion, and vortex magnetic states are plotted as functions of magnetic field in Fig. 6. From this figure, the magnetic transition occurs between two saturating SD states via the formation of an onion state at intermediate field and a vortex magnetic state near zero field. For a small ring, excitation of the vortex

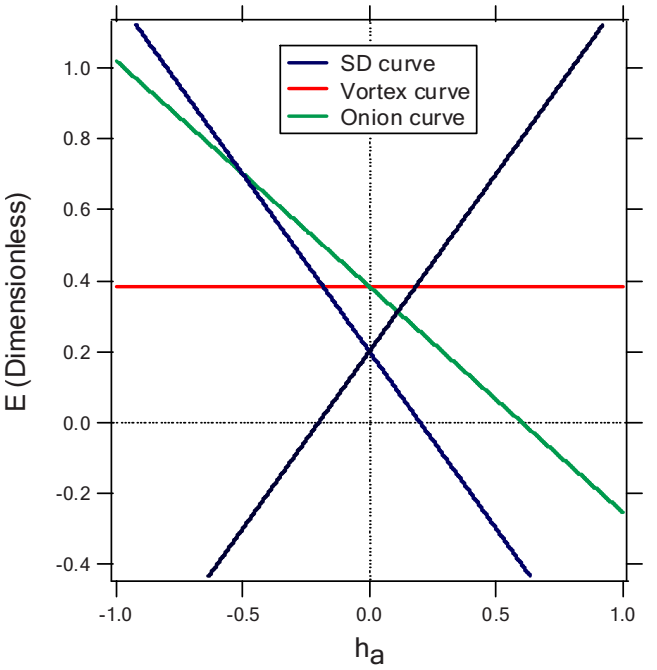

FIG. 5. (Color online) Magnetic energies of ultra-small rings. Energies of SD, vortex, and onion states are plotted as functions of dimensionless applied field h_a. (The onion curve is a lower limit—see text.)

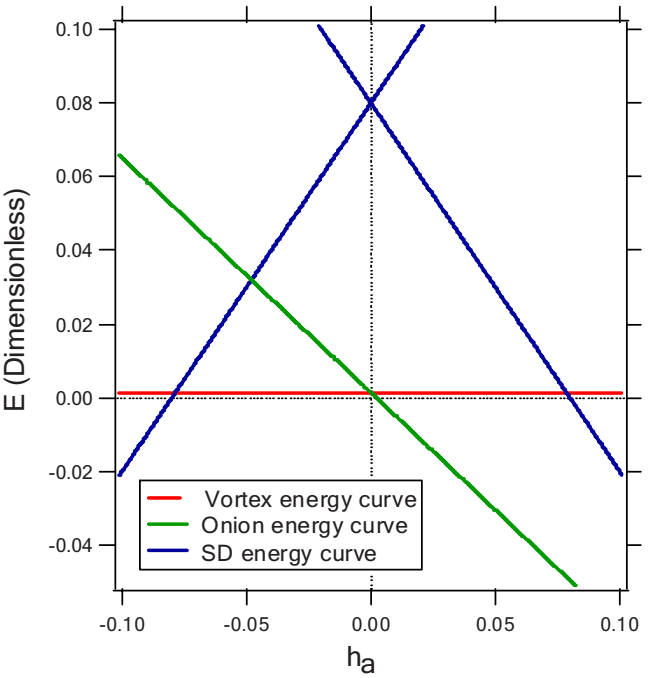

FIG. 6. (Color online) Energy plot for a small ring of diameter 150 nm, width 5 nm, and thickness 5 nm. For such a ring, the magnetic transition occurs via the formation of onion state, and finally to vortex state near zero field.

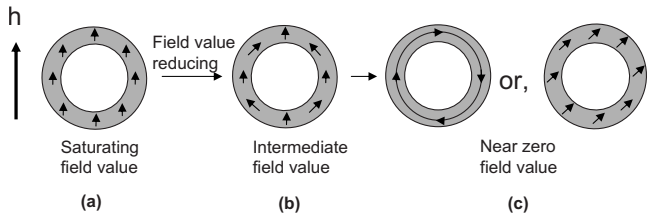

FIG. 7. (a) At very high-field value, the magnetic state of ring is single domain. (b) When the field is reduced then possible magnetic state may be a distorted SD state. (c) Near zero-field value, the magnetic state of an ultra-small ring can be either a vortex state or, rotated single domain (SD).

magnetic state is primarily due to the dominance of the magnetostatic energy term in the overall energy.

In the previous paragraphs, we discussed the energies of possible magnetic states for two magnetic rings of different lateral dimensions. It was found that the magnetic transition processes in these rings are different. At sufficiently high applied field the magnetization is saturated and the ring's magnetic state is pure single domain. As the field is reduced from its saturation value, the ring's magnetic state may no longer be purely single domain. The pure single-domain state will distort in order to minimize the total energy, which includes magnetostatic, exchange, and Zeeman energy terms. Near zero field, these competing energy terms determine the magnetic state of the ring and thus the magnetic transition process. Similarly, if the original magnetic state of a ring were a pure vortex state (for example at zero field) then changing the applied field would distort the vortex state which would eventually become a pure single-domain state at saturation. Then an important question arises: are these intermediate (distorted) magnetic states stable i.e., lower in energy than the pure SD and vortex states, respectively.

In Sec. IV, we calculate the energies of distorted SD and vortex states using a reasonable model of magnetization distortion in an ultra-small magnetic ring. It is found that small distortions in the pure SD and vortex states lead to higher energy distorted magnetic states; pure SD states are always the lowest energy magnetic states in an ultra-small magnetic ring.

IV. DISTORTED SINGLE-DOMAIN AND VORTEX STATES

For an ultra-small ring, at very high applied field the magnetic state is a saturated single domain (pure SD state). When the field is reduced from the saturation value, the pure SD state becomes distorted. A schematic description of this phenomenon is shown in Fig. 7. In this figure, we call the magnetic state at intermediate field value as the "distorted single-domain state." Figure 8(a) shows how the spin direction β depends on the azimuthal angle ϕ specifying positions along the circumference of the ring. At position ϕ, $\beta(\phi)$ is the angle between the direction of the spin and the direction of the applied field (the X axis).

It is assumed that the magnetization direction in a ring does not vary in the radial direction. Thus all the magnetic spins at a given ϕ point in the same direction β with respect

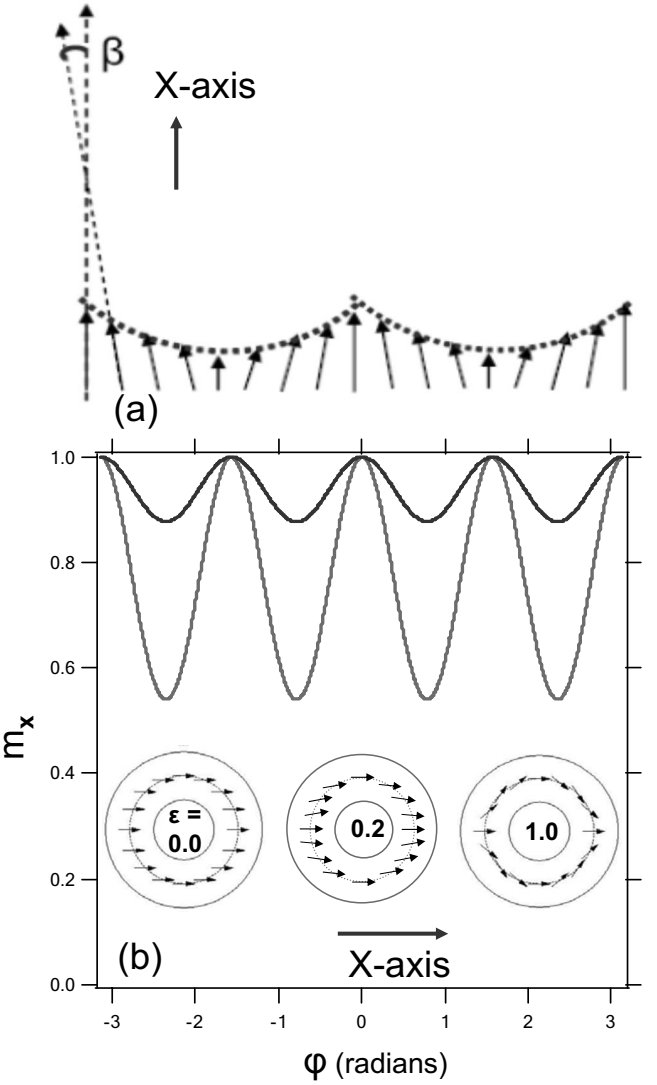

FIG. 8. (a) The one-dimensional profile of magnetic spins in a distorted SD state. $\beta(\phi)$ is the angle between a spin at azimuthal angle ϕ and the applied field axis (X axis). In this model, the angle β is supposed to be slowly varying along the circumference of the ring. (b) In this picture, m_x is plotted as a function of ϕ for two different values of distortion parameter $\varepsilon=0.2$ (dark gray curve) and 0.5 (light gray curve). Magnetic spin arrangements on the circumference of a ring for different values of distortion coefficients (0.0, 0.2, and 1.0) are shown in the inset.

to the direction of applied field. Both β and ϕ are in the range 0 to 2π (or $-\pi$ to π). It will be assumed that in the distorted single-domain state β varies only slowly with ϕ. We seek a function, $\beta=f(\phi)$, which will give us a magnetization distribution as shown in the profile of Fig. 8(a). Keeping in mind that the profile of magnetic spins shows oscillatory behavior, we chose the following function for the variation in angle β as a function of azimuthal angle ϕ:

$$\beta(\phi) = -\varepsilon \sin(2\phi), \tag{5}$$

$$m_x(\phi) = \cos[\beta(\phi)] \tag{6}$$

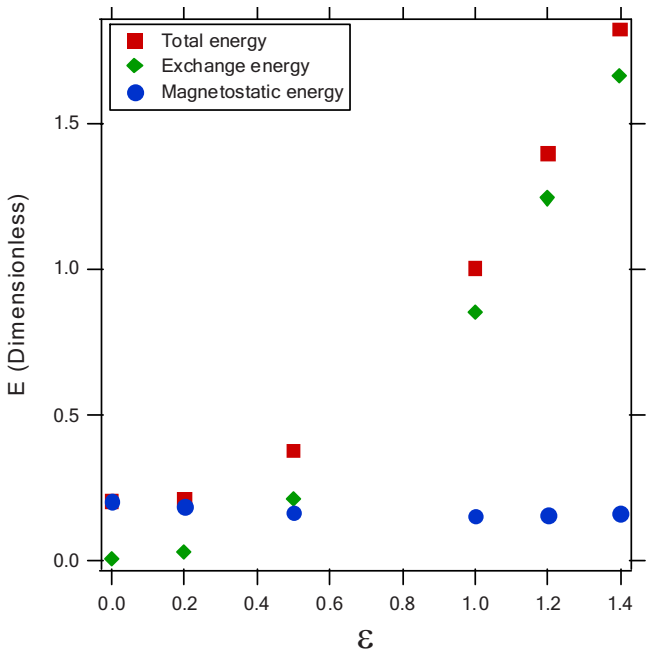

FIG. 9. (Color online) Energies of pure and distorted SD states for an ultra-small magnetic ring are plotted in this figure as a function of distortion coefficient ε.

$$=\cos(-\varepsilon \sin(2\phi)), \tag{7}$$

where ε is the distortion coefficient and X is the direction of the externally applied magnetic field. The saturated single-domain state is described by $\varepsilon=0$, with the vector **m** being in the direction of applied field. It is assumed that in the distorted state the directions of the magnetization vectors are no longer along the X axis, but their magnitudes are unchanged. Figure 8(b) shows m_x as a function of ϕ for two different distortion parameters $\varepsilon=0.2$ and 0.5. The corresponding spin directions along the circumference of a ring are as shown in the inset of Fig. 8(b). The distortion described by Eqs. (5) and (6) would appear to be a plausible one.

In zero applied field, the total dimensionless energy, $E(\varepsilon)$, of a distorted SD state is the sum of two terms.

$E(\varepsilon)=E_{ex}(\varepsilon)+E_{ms}(\varepsilon)$ (As mentioned in Sec. III, we ignore the crystalline anisotropy term in the expression for the total energy). Exchange and magnetostatic energies have been calculated as a function of distortion coefficient (ε) for the ultra-small ring geometry. In Fig. 9, exchange energy, magnetostatic energy, and total energy are plotted as a function of distortion coefficient, ε. As we see in this figure, in the pure SD state ($\varepsilon=0$) the exchange energy is minimum (zero) but the magnetostatic energy is maximum (for positive ε). With increasing distortion, the exchange energy increases but the magnetostatic energy decreases. Overall, the total energy of distorted SD state increases with increasing value of ε. We conclude that for perturbations of this particular form, at zero applied field the minimum-energy state is still a pure SD state.

Exchange, magnetostatic, and Zeeman energies depend on ε in the case of a distorted single-domain state, and ε depends on the applied field. Near zero field, the total energy is found to be minimum for ε very close to zero. So even in the presence of an applied field, pure SD state is still of lower energy than the distorted SD states. For different values of ε (pure and distorted SD states), the total energy of an ultra-small ring is plotted in Fig. 10 as a function of applied magnetic field. Our calculations suggest that distorted states with ε greater than zero are always higher in energy than the pure SD state. Perhaps the magnetization does distort, but to some other shape, that we did not take into account.

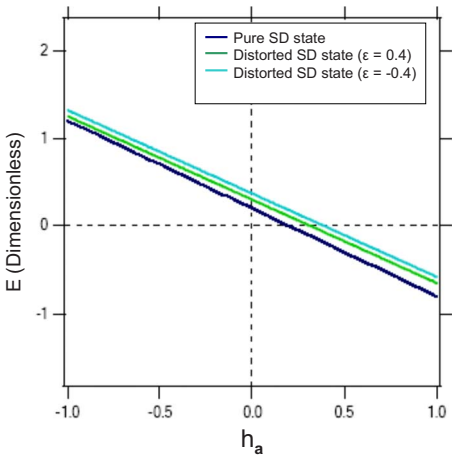

FIG. 10. (Color online) In this figure, energies of pure SD state and distorted SD states are plotted as a function of field.

Now we want to check whether or not distortion in a pure vortex state leads to a state of lower energy. A possible scenario is that near zero field the magnetic state of an ultra-small ring is already a vortex state and that as the applied field changes the ring makes a transition to a saturated single-domain state via the formation of distorted vortex state. For this purpose, we consider another realistic model that involves a vortex distortion coefficient, ε_v. In this model, the vortex magnetization state is given by

$$m_x = \cos(\beta),$$

$$\beta(\phi) = \frac{\pi}{2} + \phi - \varepsilon_v \cos(\phi), \tag{8}$$

where once again $\beta(\phi)$ is the angle between the direction of the magnetization vector and the field direction (applied along the X axis). $\varepsilon_v=0$ corresponds to no distortion and $\beta(\phi)=\pi/2+\phi$. Again the total energy of an ultra-small ring in zero field consists of exchange and magnetostatic energy terms (ignoring the magnetocrystalline anisotropy energy term). For distorted vortex states the exchange energy as a function of ε_v is given by the following equation:

$$E_{ex}(\varepsilon_v) = \frac{(1/2)l_{ex}^2}{\pi(R_2^2 - R_1^2)} \pi(2+\varepsilon_v^2) \ln\frac{R_2}{R_1}. \tag{9}$$

Magnetostatic energies for distorted vortex states are calculated by numerical integrations (as explained previously). In Fig. 11, we have plotted the total energy of distorted vortex states in zero field as a function of vortex distortion coefficient ε_v. As we see in this figure, the pure vortex state is

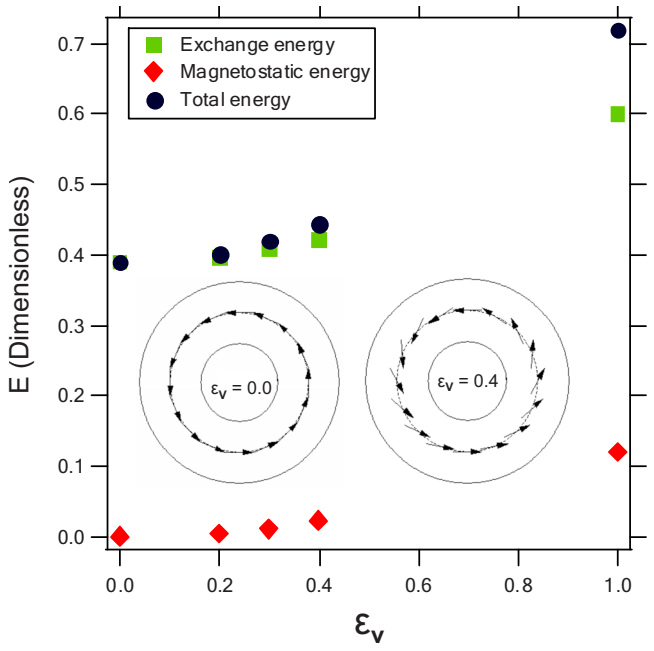

FIG. 11. (Color online) Energies of pure and distorted vortex states, in zero field, are plotted in this figure as a function of distortion coefficient ε_v. Magnetic spin arrangements on the ring's circumference for two different values of distortion coefficients (0.0 and 0.4) are also shown in the inset.

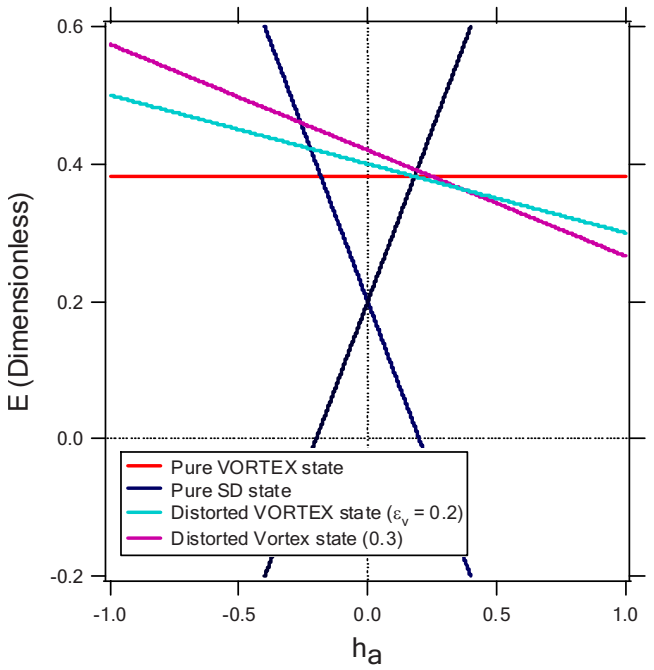

FIG. 12. (Color online) This plot shows total magnetic energies of pure and perturbed vortex magnetic configurations (red, light blue, and purple lines), together with the energy of the pure SD state (dark blue line) as a function of applied field. Pure SD state is always the lowest energy state.

the lowest energy state in zero field. In the following paragraph we will compare the energies of pure and distorted vortex states in the presence of a changing applied field.

In the presence of a field, the total energy consists of three terms,

$$E(\varepsilon_v) = E_{ex}(\varepsilon_v) + E_{ms}(\varepsilon_v) + E_{zeeman}(\varepsilon_v).$$

Zeeman energy for distorted vortex states is given by

$$E_{zeeman}(\varepsilon_v) = -\frac{h_a}{2\pi} 2\pi BesselJ[1, \varepsilon_v]. \quad (10)$$

Total energy, including the Zeeman energy, for pure and distorted vortex states (for distortion parameters ε_v=0.2 and 0.3), along with the total energy of pure SD states, are plotted in Fig. 12 as a function of applied field. Some interesting behaviors are observed in this figure.

Near zero field, pure vortex state is still the lowest energy state. At a field value of 0.2 or so the state with distortion ε_v=0.2 (light blue) crosses over to become lower in energy than the state with distortion ε_v=0.0. At a somewhat higher field the purple curve with distortion parameter ε_v=0.3 becomes the one with lower energy. This is not exactly the case for distorted SD states (Fig. 10), as discussed earlier. In the case of single-domain states, pure SD states always remain the lowest energy states as the applied field is changed. Therefore distorted single-domain states can be ignored in considering the magnetic transition in an ultra-small magnetic ring. Thus there are three important states to consider: pure SD state, pure vortex state and distorted vortex state. As inferred from Fig. 12, it is concluded that pure SD states are always the lowest energy states.

V. DISCUSSION

Based on the above analysis, it is found that the magnetic transition process for ultra-small ring would involve pure SD states of opposite polarity and the transition occurs via the rotation of SD state. Similar calculations for small rings suggest that the magnetic transition process in this case would be from one SD state to another SD state of opposite polarity via the formation of onion state at intermediate field and pure vortex state near zero field (Fig. 6). In the experimental data for small ring [Fig. 4(a)], we see that the magnetic transition starts occurring around ~1000 Oe of field value but the curvature of magnetic transition is very large.

We have verified our calculations using micromagnetic simulations. Simulations were carried out for both ultra-small and small ring geometries and were computed by solving the micromagnetic equilibrium equation for each applied field on a square mesh, with a 0.1 nm cell size for ultra-small ring and 2 nm for small ring. The OOMMF package[20] was used for the micromagnetic simulations. The intrinsic parameters used for Co are: $M_s = 1400 \times 10^3$ A/m, $A = 17 \times 10^{12}$ J/m, and $K_1 = 0$. Micromagnetic simulation results are shown in Fig. 13 and are in reasonably good agreement with our energetic analysis. Figure 13(a) shows that the magnetic transition in an ultra-small ring occurs via the uniform rotation of SD state. In a small ring, the magnetic transition process involves the formation of vortex magnetic state and the onset to vortex state transition starts at ~1000 Oe.

The above analysis and micromagnetic simulations reasonably explain the magnetic transition process in a small ring. In the case of an ultra-small ring, however, the experi-

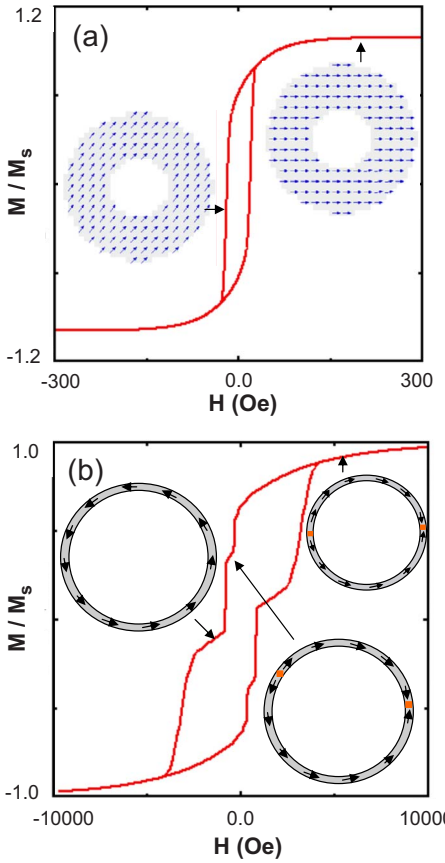

FIG. 13. (Color online) (a) Micromagnetic simulated magnetic hysteresis loop for ultra-small ring. Magnetic transition process in an ultra-small ring occurs between pure SD states via the uniform rotation of spins. (b) Hysteresis loop generated using micromagnetic simulations for small ring. In this case, magnetic transition occurs via the formation of vortex magnetic state near zero field.

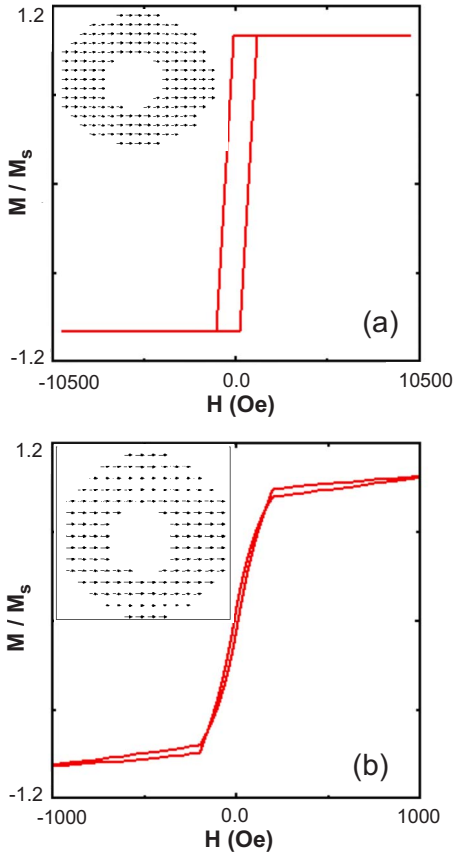

FIG. 14. (Color online) (a) Magnetic hysteresis curve generated using micromagnetic simulations for slightly asymmetric ultra-small ring (outer diameter=14 nm along X axis and 12 nm along Y axis). The magnetic transition occurs between pure SD states of opposite polarity. (b) Simulated hysteresis curve for another slightly asymmetric ultra-small ring (outer diameter=12 nm, distorted along Y axis).

mental data [Fig. 3(a)] is not quite the same as expected from the energy calculations. The explanation for this discrepancy lies in the variation in shapes and sizes of ultra-small rings (outer diameter varies between 12–14 nm). Due to the ultra-small nature of these magnetic elements (as compared to exchange length), even a slight distortion in the shape and size causes a change in the magnetic transition process of individual element. To illustrate this fact, we have performed micromagnetic simulations using the same intrinsic parameters (M_s and A) for two different ultra-small rings: in first case, the outer diameter of the ring is 14 nm along X axis and 12 nm along Y axis and in second case, the outer diameter of ring is 12 nm with a slight distortion along Y axis. The simulation results are shown in Fig. 14. In both cases, magnetic transition occurs via the rotation of an SD state, vortex state does not form. In this figure, we clearly see that small changes in the shape and size of an ultra-small ring strongly affect the magnetic transition process. In the magnetic hysteresis measurements, we observe the collective behavior of an array. Since magnetic rings of different shapes and sizes behave differently, the observed magnetic hysteresis curve appears different than the calculated one for a perfect ultra-small ring. It is also possible that this variation in the shapes of ultra-small rings may lead to interring interactions. More theoretical works are necessary to further understand it. Earlier, Cowburn *et al.* studied the magnetic transition in small magnetic disk arrays and established that the magnetic transition occurs between pure SD states.[21]

Magnetic measurements at room temperature for both ultra-small and small rings do not show any magnetic hysteresis. At high temperature, thermal fluctuations dominate the magnetic energy of these rings. This cancels out any remnant magnetization at zero field. In the low-temperature magnetic hysteresis curve for ultra-small ring arrays [Fig. 3(a)], there is a slight asymmetry between positive and negative fields. This is possibly due to a weak exchange bias phenomenon. On the surface of the ring, partial oxidization of Co material into CoO creates an interface of ferromagnetic (FM) (Co)/antiferromagnetic (AFM) (CoO) layer, resulting in a very weak exchange bias phenomenon. Similar behavior has recently been reported in small ferromagnetic disks.[22]

Now we summarize the above analysis for ultra-small and small ring geometries: a magnetic ring's geometrical parameters and the exchange length of the parent magnetic material decide which magnetic state has the lowest energy at zero field. Increasing the diameter reduces both the magnetostatic

and exchange energies but the exchange energy decreases more rapidly and therefore magnetostatic energy starts dominating as the overall diameter of the magnetic ring increases. In the above analysis it has been assumed that for both small and ultra-small rings the magnetization pattern is purely two-dimensional (2D); the magnetization vector does not cant out of the ring's plane. For a magnetic ring of width and thickness comparable to the characteristic length (exchange length) of the parent magnetic material, this assumption is quite reasonable. As a consequence, we do not observe the "triple point"—defined as the point where the energies for onion, vortex, and uniform out-of-plane magnetization are same—as recently reported by other authors based on theoretical calculations for the ring geometry.[23,24]

To have a complete understanding of these magnetic transition phenomena, one needs to solve the following integrodifferential equation[25,26]:

$$l_{ex}^2 \frac{d^2\beta}{d^2\phi} + \cos(\beta)\rho^2 h_M - \sin(\beta)\rho^2 h_M - \sin(\beta)\rho^2 h_{ax} = 0,$$

$$h_M(\rho,\phi) = \int d\phi' \sigma(\beta,\phi') K(\rho,\phi,\phi'), \tag{11}$$

where ρ is the radial coordinate, σ is magnetic pole density (depending on azimuthal position ϕ'), the kernel K is an explicit but complicated function involving ρ and ϕ and X is the direction of applied magnetic field. By solving these integrodifferential equations, we can get the functional $\beta(h,\phi)$ and since $m(h)=\cos\beta$, $(m=1)$, so we can get m (magnetization) as a function of h (dimensionless magnetic field). Future works discussing the solution of above integrodifferential equations would be very desirable.

ACKNOWLEDGMENTS

This project was supported by NSF Grants No. DMR-0531171 and No. DMR-0306951, and MRSEC.

[1] Y. G. Yoo, M. Klaui, C. Vaz, L. Heyderman, and J. Bland, Appl. Phys. Lett. **82**, 2470 (2003).
[2] M. Kläui, C. A. F. Vaz, L. Lopez-Diaz, and J. A. C. Bland, J. Phys.: Condens. Matter **15**, R985 (2003).
[3] M. Natali, I. L. Prejbeanu, A. Lebib, L. D. Buda, K. Ounadjela, and Y. Chen, Phys. Rev. Lett. **88**, 157203 (2002).
[4] J. G. Zhu, Y. Zheng, and G. A. Prinz, J. Appl. Phys. **87**, 6668 (2000).
[5] J. Rothman, M. Klaui, L. Lopez-Diaz, C. A. F. Vaz, A. Bleloch, J. A. C. Bland, Z. Cui, and R. Speaks, Phys. Rev. Lett. **86**, 1098 (2001).
[6] R. Skomsky, *Spin Electronics* (Springer Publishing Group, New York, 2000), Chap. 10.
[7] R. P. Cowburn, J. Phys. D **33**, R1 (2000).
[8] A. Aharoni, Phys. Rev. B **45**, 1030 (1992).
[9] J. M. D. Coey, *Spin Electronics* (Springer Publishing Group, New York, 2000), Chap. 12.
[10] L. J. Heyderman, C. David, M. Klaui, C. Vaz, and J. Bland, J. Appl. Phys. **93**, 10011 (2003).
[11] F. Q. Zhu, G. Chern, O. Tchernyshyov, X. Zhu, and J. Zhu, Adv. Mater. **16**, 2155 (2004).
[12] K. L. Hobbs, P. Larson, G. Lian, J. Keay, and M. Johnson, Nano Lett. **4**, 167 (2004).
[13] A. Kosiorek, W. Kandulski, H. Glaczynska, and M. Giersig, Small **1**, 439 (2005).
[14] D. K. Singh, R. Krotkov, H. Xiang, T. Xu, T. Russell, and M. Tuominen, Nanotechnology **19**, 245305 (2008).
[15] T. Albrecht, J. DeRouchey, C. Stafford, E. Huang, M. Bal, M. Tuominen, and T. Russell, Adv. Mater. **12**, 787 (2000).
[16] M. Bal, A. Ursache, J. Goldbach, T. Russell, and M. Tuominen, Appl. Phys. Lett. **81**, 3479 (2002).
[17] M. Klaui, C. Vaz, J. Bland, and L. Heyderman, Appl. Phys. Lett. **85**, 5637 (2004).
[18] S. P. Li, D. Peyrade, M. Natali, A. Lebib, Y. Chen, U. Ebels, L. D. Buda, and K. Ounadjela, Phys. Rev. Lett. **86**, 1102 (2001).
[19] M. Bertotti, *Hysteresis and Magnetism* (Academic Press, New York, 1998).
[20] The public domain package is available at gams.nist.gov/oommf
[21] R. P. Cowburn, D. K. Koltsov, A. O. Adeyeye, M. E. Welland, and D. M. Tricker, Phys. Rev. Lett. **83**, 1042 (1999).
[22] J. Sort, K. S. Buchanan, V. Novosad, A. Hoffmann, G. Salazar-Alvarez, A. Bollero, M. D. Baro, B. Dieny, and J. Nogues, Phys. Rev. Lett. **97**, 067201 (2006).
[23] V. P. Kravchuk, D. Sheka, and Y. Gaididei, J. Magn. Magn. Mater. **310**, 116 (2007).
[24] P. Landeros, J. Escrig, D. Altbir, M. Bahiana, and J. Castro, J. Appl. Phys. **100**, 044311 (2006).
[25] W. F. Brown, *Micromagnetics* (Wiley, New York, 1963).
[26] A. Aharoni, *Theory of Ferromagnetism* (Oxford Science Publication, Oxford, UK, 2000).